

Article

The Influence of Bearing Clearance on the Load Capacity of Gas Polymer Bearings

Gregor Schilling  and Robert Liebich * 

Department for Engineering Design and Product Reliability, Technical University of Berlin,
Straße des 17. Juni 135, 10623 Berlin, Germany

* Correspondence: robert.liebich@tu-berlin.de

Abstract: In this paper, the influence of a nominal bearing clearance on the lift-off behaviour and the load-carrying capacity of gas polymer bearings (GPBs) is investigated. For this purpose, an experimental study with five different bearing gap configurations and a range of static loads is carried out. Furthermore, the test rig for the clearance and friction torque measurements is illustrated and discussed from a practical point of view. The experimental gap measurement results of all the bearing configurations and the method used are explained and discussed. Finally, the friction torque during the lift-off and run-up phases is measured for a range of static loads. A method that uses the time derivative of the measured friction torque during the run-up tests as a criterion for the lift-off detection is explained and applied to the measured data. The results of this study indicate that there are large differences between the most studied bump-type and gas polymer bearings in terms of the dependence of the load-carrying capacity on the bearing gap. Furthermore, the recorded effects are described, and possible explanations are given. Finally, the differences in characteristics from those of bump-type bearings are described and their importance for the design process of rotors supported in GPBs is explained.

Keywords: load capacity; gas polymer bearing; gas foil bearing; bearing clearance; lift-off



Citation: Schilling, G.; Liebich, R. The Influence of Bearing Clearance on the Load Capacity of Gas Polymer Bearings. *Appl. Sci.* **2023**, *13*, 4555. <https://doi.org/10.3390/app13074555>

Academic Editor: Marco Troncosi

Received: 3 March 2023

Revised: 26 March 2023

Accepted: 1 April 2023

Published: 3 April 2023



Copyright: © 2023 by the authors. Licensee MDPI, Basel, Switzerland. This article is an open access article distributed under the terms and conditions of the Creative Commons Attribution (CC BY) license (<https://creativecommons.org/licenses/by/4.0/>).

1. Introduction

One of the main objectives in the development of future-proof machinery is to enhance efficiency, both from an economic and ecological standpoint. Simplifying systems in general, while simultaneously reducing operating resources and maintenance during operation, can offer significant benefits. In the field of fast-rotating rotors, improvements in bearing technologies can serve as a potential starting point for increasing efficiency. The implementation of aerodynamic bearings represents a particularly promising approach to tackling these challenges, as they possess a straightforward design and do not require lubricants. As a result, auxiliary components such as pumps and supply systems can be eliminated. However, due to the lower viscosity of gases, these bearings are associated with reduced load capacities when compared to those of hydrodynamic oil bearings. To address these drawbacks and enhance the performance of aerodynamic bearings, gas foil bearings have been developed. Another advantage of the elastic structure is that additional damping is provided to the rotor through energy dissipation, which occurs through friction within the elastic structure.

Unlike conventional air bearings, gas foil bearings have a compliant support structure instead between the bearing bore and their housing. Due to the interaction between the supporting pressure field and the elastic bearing wall, a self-optimized gap geometry can be reached. As a result, higher load capacities and an improved stability behaviour can be achieved [1,2]. There are several different parameters that have an impact on the load-carrying capacity of these bearings. In addition to the stiffness properties of the elastic support structure, both the shape and the size of the bearing gap are important design parameters, with respect to the achievable load capacity.

The most investigated variant of gas foil bearings is the bump foil or bump-type bearing. In 2002, Radil et al. [3] published their performance results of a clearance study for a bump-type bearing with an axially split bump foil. For this purpose, they defined a bearing coefficient in the form of a measure for the maximum load that is bearable, depending on the bearing's length and diameter as well as the shaft speed. The presented test method used a shaft that ran at a constant speed. A load was then applied and increased until the measured frictional torque increased significantly. The results showed that an optimal range for clearance in terms of the load capacity does exist. The data also showed a rapid decrease in the capacity when the air gap becomes too small.

Another measurement of the lift-off speed as a performance measure was presented by San Andrés et al. [4] in 2012. In this work, the authors compared the performance of a metal mesh foil bearing and that of a common bump-type bearing. For this comparison, among other aspects, the lift-off speed and the maximum starting torque were used. In contrast to the work of Radil et al. [3], a different method was used in this paper. San Andrés did not investigate the load capacity by increasing the load at a constant speed. Instead, several transient rotor run-ups were performed, and the frictional torque was measured. The lifting point was then determined based on a subjective limit for the frictional torque. Further lift-off and drive torque measurements were presented by Rudloff et al. [5]. The presented test rig uses an elastic bearing mount (squirrel cage) instead of a free-floating housing. The bump-type bearing was placed in a rolling bearing, while the torque was transmitted via a lever connected to a force gauge. The presented friction torque characteristic is like that published by San Andrés. When the shaft is accelerated beyond the lift-off speed, the torque drops rapidly until only air friction remains. It is notable that the transient signal of the torque displays a minimum after the lift-off event has occurred. A very similar behaviour is presented by San Andrés et al. [6]. The measured drive torque of the investigated metal mesh bearing also shows a minimum after lift-off. This minimum was used as a criterion for the lift-off determination.

So far, only a few researchers have published studies on gas foil bearings with a polymeric elastic structure. In 2004, Hou et al. [7] compared two kinds of elastic foil structures for a small cryogenic turbo-expander. The application of rubber as a compliant wall component showed preferable damping and stability characteristics. Later, in 2004, Hou et al. [8] published another investigation on a compliant foil bearing with a polymeric structure. The authors mentioned that the bearings also showed a superior dynamic behaviour and stability performance in the tested speed range up to 150 krpm ($15.7 \cdot 10^3$ rad/s). A hybrid gas foil bearing was the subject of an investigation by Lee et al. [9]. Their rotordynamic test rig consisted of a flexible rotor in gas foil bearings with a bump foil and an acrylic polymer layer between the bump and top foils. The study compared the stiffness and damping characteristics with and without the polymer. It was shown that the hybrid bearing had a similar or slightly higher stiffness, but a significantly increased damping capacity. The rotor amplitudes could be considerably reduced using a polymer layer, especially in the range of the natural frequencies and in supercritical operation.

Another performance study was conducted in 2017 by Sim and Park [10], comparing the structural and rotordynamic behaviour of a conventional bump foil bearing, a hybrid version with a bump foil and polymer, and a gas polymer bearing. The experimental dynamic analysis for all three types of compliant structures also demonstrated the higher damping potential of the polymeric foil bearings. In addition, the appearance of subharmonic vibrations during the rotordynamic tests was also shifted to higher rotational speeds, and the reached amplitude level was significantly lower. In 2022, a further rotordynamic study from Park et al. [11] confirmed the beneficial damping behaviour of foil bearings with viscoelastic material (in this case: nitrile butadiene rubber—NBR) as part of the compliant bearing wall. In addition to experimental investigations, several numerical studies have already been carried out on the structural modelling of the polymers used (e.g., [12,13]).

The studies on gas polymer bearings presented so far have investigated the bearing behaviour in terms of subharmonic vibrations and stability, or structural modelling. The

lift-off behaviour and load-carrying capacity of gas foil bearings are also important performance criteria for the application of this bearing technology. This paper experimentally investigates the load-carrying capacity of gas foil bearings with a polymeric, compliant structure. For this purpose, a GPB prototype was manufactured and its design is illustrated and described. The results of the bearing clearance measurements are then presented. Finally, the results of the lift-off speed and load capacity investigations are presented and discussed.

2. Materials and Methods

2.1. Bearing Prototype Assembly

In Figure 1, the assembly of the GPB prototypes is presented. The rigid housing of the bearing is made of aluminium with an outer diameter of 40 mm. The overall length of the bearing is 25 mm. The area where the foils and the polymer layer are placed is shorter than the housing. The resulting shoulders are used to mount two spring washers on both sides as a stop in the axial direction. The seat for the polymer and the foils is 0.5 mm longer than the axial length ($L = 20$ mm) of the used polymer sheet and the metal foils. This additional clearance in axial direction is provided to avoid deformation restrictions at the edges of the unconstrained polymer layer. The height of these shoulders has to be high enough to ensure that the axial movement of the rubber is restricted but it has to be low enough to avoid physical contact between the rotor and the spring washer. For the determination of the shoulder height, the stiffness of the polymer and the possible radial deformation due to the pressure field have to be considered. The inner diameter of the washer is 1 mm smaller than the seat of the polymer and adjustment foil, resulting in a stop height of 0.5 mm. With an NBR layer thickness of about 2 mm, the shoulder height is less than or equal to a quarter of the height of the rubber and adjustment foil. The elastic polymer structure is made of nitrile butadiene rubber (NBR) with a hardness of 50 ± 5 Shore A. The layer has a nominal thickness of 2 mm and a width of 20 mm. The rubber is loosely placed on its seat and not fixed at any edge. Thin metal sheets between the housing and the polymer are used to adjust the nominal radial clearance between the bearing and the shaft. In this study, high precision adjustment foils with a thickness of 20, 50, 75, and 100 μm were used to reduce the radial clearance. The top foil of the test bearings, as well as the adjustment foils, has a thickness of 50 μm and is made of stainless steel. A borehole that slightly cuts the polymer seat of the housing was provided to fix the top foil on one edge via clamping.

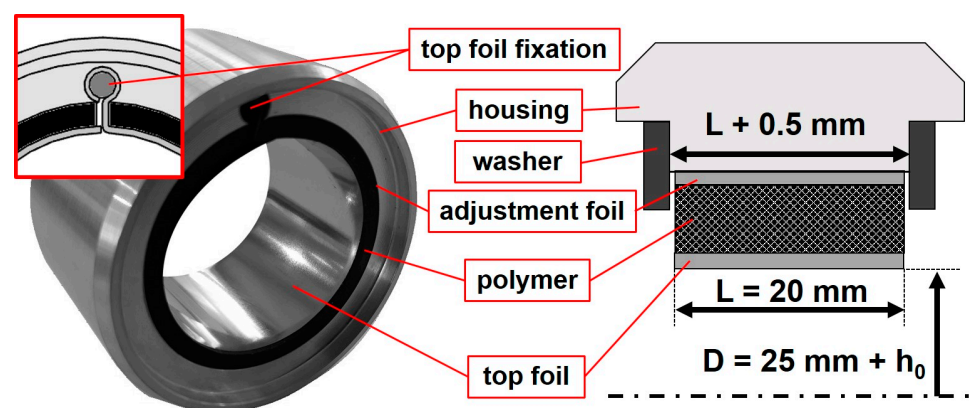


Figure 1. Assembly of the gas polymer bearing with adjustment foils; left: test bearing, right: schematic cross section of the GPB.

2.2. Nominal Clearance Test Rig

To determine the nominal clearance of the tested GPB configurations, a commonly used force–displacement-based test setup was designed. Most test setups found in the literature use a lathe or a fixed shaft and horizontal bearing motion [14–16]. Figure 2 shows a picture of the test rig that is used in this paper. The bearing is placed on the pedestal, with

six angular positions for force application and displacement measurement. The additional horizontal movement of the bearing pedestal is generated by a positioning table with two axes. The second axis of the table is used for height adjustment. Unlike other published test facilities, the connection between the movable component (here: the positioning table) and the bearing pedestal is not realized directly via the force sensor. Instead, an elastic stinger is used to reduce the influence of misalignments or manufacturing deviations to the measurement. The pedestal is supported by linear roller bearings to reduce friction in its bottom plane. The shaft is oriented vertically. This avoids bending moments caused by gravity, which would affect the force measurement. The same shaft is later used to measure the friction torque to ensure that the determined clearances are valid and do not vary due to manufacturing tolerances. The measuring procedure starts with the movement of the positioning table, which also moves the bearing pedestal via the stinger. When the movement exceeds the bearing gap, the elastic structure inside the bearing is pressed against the fixed shaft, resulting in a rapidly increasing reaction force. This resistance is detected by the force sensor. This procedure has to be executed in both directions to determine the low force displacement range without physical contact between the compliant structure and the fixed rigid shaft. It should be noted that the displacement sensor is located on the opposite side of the force application point, instead of the positioning table, to ensure that only the stiffness characteristics of the compliant bearing structure are measured. The force–displacement curves generated in this way can then be used to determine the radial bearing clearance by applying different methods to the measured data.

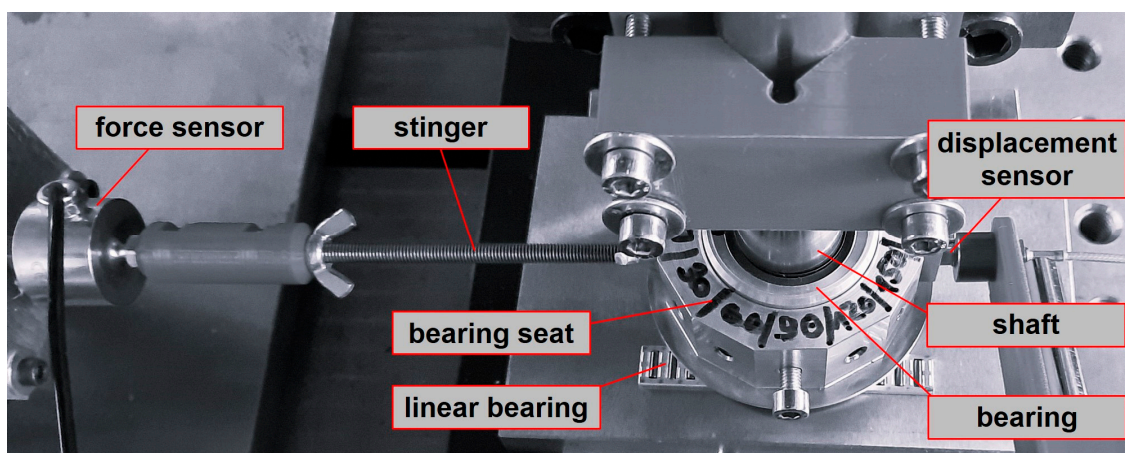


Figure 2. Illustration of the test rig for clearance measurements.

The most commonly used method for determining the nominal clearance uses the rapid increase in the reaction force after the air gap is exceeded. Here, either the force–displacement curve is used directly or its derivative (the stiffness–displacement curve) is used. Regarding the rapid but not instantaneously increasing force, a threshold value for the force or the stiffness has to be defined. Both variants have been used in the past by other research groups, e.g., the force-based version in [3,11] and the stiffness curve version in [10,14,15]). The distance between the intersection points of the measured data and the threshold level corresponds to twice the bearing gap. It should be noted that the definition of the threshold stiffness used in this paper, as well as in the referenced papers, is subjective and based on a visual evaluation of curves in Section 3.1. Of course, the choice of the level has an influence on the determined bearing gap. How strong this influence is depending on the force or stiffness gradient. However, the threshold established in this study is the same for all bearing configurations tested, allowing for comparability between results.

2.3. Rotor Lift-Off Test Rig

The design of the friction torque and lift-off speed setup presented in Figure 3 and described in the following is similar to other published setups, e.g., [3,4,6]. As mentioned earlier, the shaft used is the same as for the clearance measurement setup. While the test bearing is placed on the front of the shaft, a 3D-printed impulse turbine is on the back side. The shaft is supported by eight ball bearings in two planes (four per plane) along the shaft. These planes are located between the turbine and the test bearing. The housing in which the ball bearings are located is open at the top and bottom, ensuring that the pressure can quickly decrease after the turbine housing, thus preventing air flow through the bearing gap.

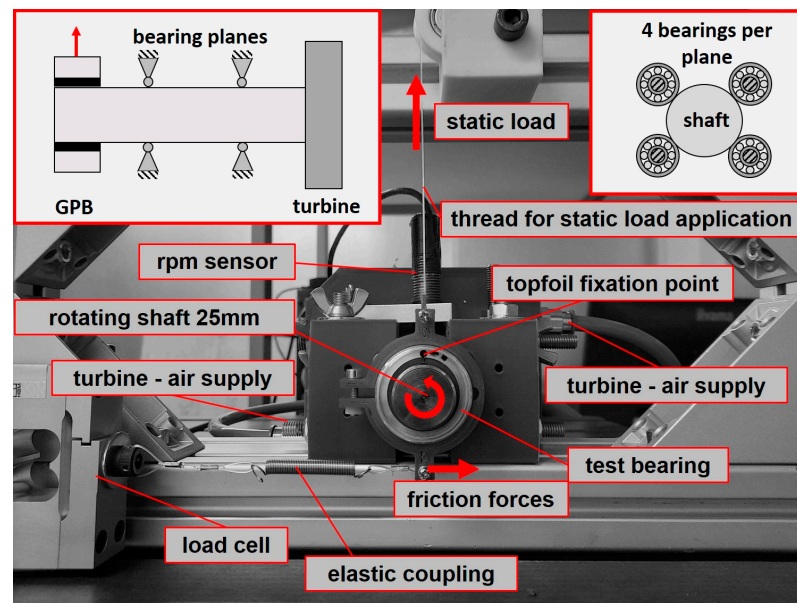


Figure 3. Illustration of the test setup for lift-off measurements.

An infrared (IR) contrast sensor is used to determine the rotational speed. The static load is applied via a tear-resistant polymer thread (connected to weights) and measured continuously with a load cell. An elastic coupling connects the force sensor, which is used to measure the frictional torque, and the bearing mount. The use of elastic couplings between the bearing seat and surrounding components allows the bearing to self-align. This can help to reduce the influence of reaction forces as a result of misalignment. Nevertheless, it should be mentioned that the setup is not designed to measure the absolute value of the friction torque. A general problem for such designs is a resulting righting moment from the static load thread and preloads from assembly. The resulting offsets are nearly unpredictable and can result in different effects, e.g., negative friction torques after lift-off if the offset is subtracted from the force signal before run-up, as shown by Rudloff et. al. [5]. To acknowledge these effects, the presented torques in this paper are normalised by their absolute maximum value.

In this study, static loads of 10, 30, 50, and 70 N are applied to each bearing configuration to investigate the lift-off behaviour. In contrast to the work of Radil [3], a transient procedure, similar to that of San Andres [4,6], is used in this study. In [6], a temperature increase of 10–18 °C was measured by San Andres, after a time period of 15 min of constant operation at a specific load, an ambient temperature of 21 °C, and a rotational speed of 65 krpm ($6.8 \cdot 10^3$ rad/s). Due to the high temperature dependency of polymeric stiffness behaviour, the overall time per test has to be as short as possible to avoid significant temperature increases during the tests. The ambient temperature during the measurements presented in Section 3.2 was between 20 and 21 °C. The amount of time for each test at a specific load was in the range of 6 to 12 s between the beginning of the rotation and its

end. A time at zero speed of at least 60–90 s for weight change and data processing passed between two measurements. Due to the extremely short time periods per test and the much longer periods out of operation between two measurements (5 to 15 times longer), the polymer as well as the whole test rig showed no significant temperature increase during the tests. Nevertheless, the temperature aspect has to be addressed and will be discussed in Section 4.

3. Results

3.1. Nominal Clearance Measurement

To determine the radial clearance, the stiffness curve over the bearing displacement is used. Note that the presented stiffness is calculated using force signals normalized to their absolute maximum value, and the offset is adjusted. This pre-processing improves the comparability within a series of measurements. The determination of the threshold value in this publication, as in the works referenced above, is subjective and in this case defined visually with respect to the graph. Figure 4 shows the measured stiffness (black crosses) for the bearing configuration without the adjustment foil.

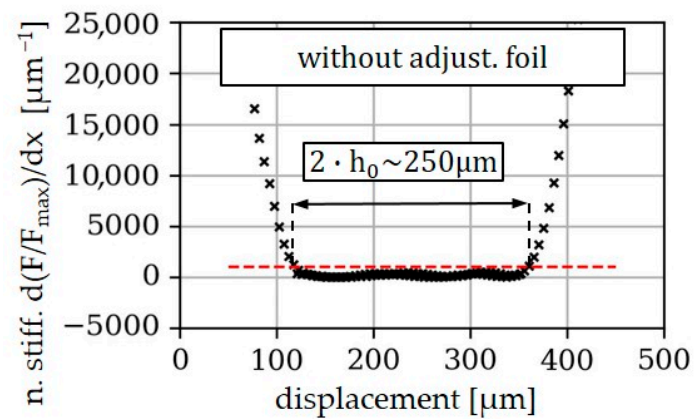


Figure 4. Example of a stiffness curve for the bearing configuration without adjustment foil at 60°–240°; position-dependent normalized stiffness (black crosses); and threshold level (red dashed line).

The graph shows a low stiffness region and a rapid increase at both ends. Due to the small residual ripple in the lower stiffness region, a threshold of $1000 \mu\text{m}^{-1}$ is defined (red dashed line) and used for all bearing configurations in this study. The total distance between the two intersecting points is approximately $250 \mu\text{m}$, which is equal to twice the radial bearing clearance. The measurement results for all the configurations with an adjustment foil are shown in Figure 5. For the thinner foils ($20 \mu\text{m}$ and $50 \mu\text{m}$) shown in Figure 5a,b, the value of the stiffness is nearly constant between the intersecting points. In contrast, the data from the thicker foil configurations ($75 \mu\text{m}$ and $100 \mu\text{m}$) do not show a constant course anymore. This effect can be attributed to the fact that the foils and the elastic material are not completely attached to the rigid inner wall of the housing. The main reason for this issue is the pre-processing of the adjustment foils. Due to the higher stiffness, the sheets with a thickness of $75 \mu\text{m}$ and $100 \mu\text{m}$ were pre-curved before installation to prevent lifting at the foils' ends. However, due to the pre-curving, the foils no longer laid as smoothly against the inner wall of the bearing. Comparable behaviour has also been measured in other publications, e.g., [14,15,17].

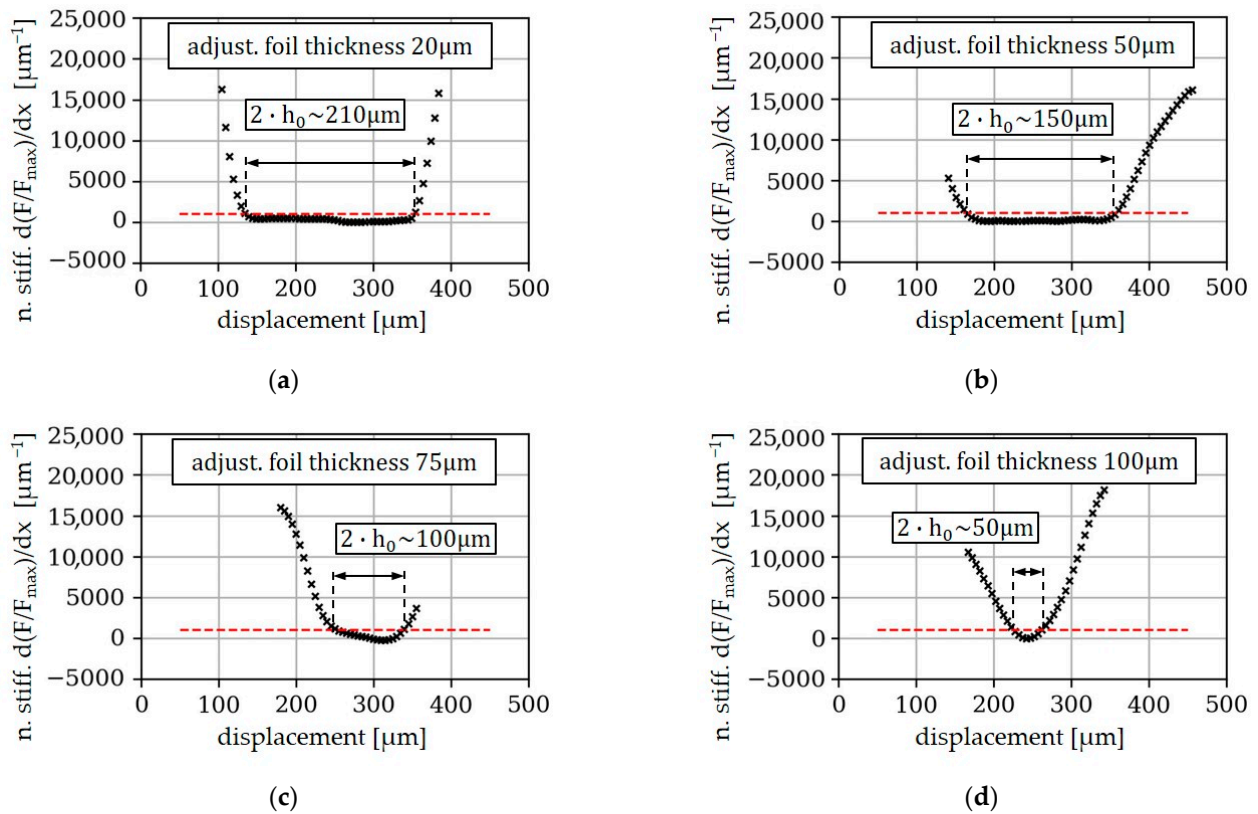


Figure 5. Results of the gap measurement for the GPB with adjustment foil at 60° – 240° ; position-dependent normalized stiffness (black crosses); threshold level (red dashed line); and adjustment foil thickness (a) $20\ \mu\text{m}$; (b) $50\ \mu\text{m}$; (c) $75\ \mu\text{m}$; (d) $100\ \mu\text{m}$.

Below the threshold level, the stiffness curve does not show a flat range, instead it shows a slope and a rise, as well as the minimum in between. Nevertheless, the gradient (incline/decline per μm displacement) of the stiffness curve also increases rapidly above the threshold. For the $100\ \mu\text{m}$ adjustment foil configuration in case (d), the difference between the curves’ gradients below and above the threshold disappears completely. However, the minimum of the curve remains below the threshold.

Table 1 shows the mean values of all the measured angular positions for all the bearing configurations, as well the mean of the maximum and minimum measured clearances. The nominal values given correspond approximately to the mean value between the maximum and minimum measured gap. At this point, the subjective choice of the threshold value should be emphasized once again since it has a significant influence on the results of the gap measurement. Due to the rapidly increasing stiffness, the absolute deviations of the results can also vary depending on the threshold value.

Table 1. Summary of the results of the bearing gap measurements.

Adjustment Foil Thickness [μm]	Mean Clearance [μm]	$(h_{\text{max}} + h_{\text{min}})/2$ Clearance [μm]	Nominal Radial Clearance h_0 [μm]
0	122.83	124.5	125
20	102.667	105.5	105
50	78.83	76.5	75
75	53.92	53	50
100	26.92	25.5	25

3.2. Run-Up Measurements

Figure 6 shows the measured transient signals of the frictional torque (black line) and the rotational speed (light grey line) for two different bearing configurations. Figure 6a corresponds to the data for the configuration with a bearing clearance of $105\ \mu\text{m}$ and a static load of 10 N. In Figure 6b, on the other hand, the dataset of a configuration with a smaller clearance ($25\ \mu\text{m}$) and a higher static load (70 N) is presented. As the turbine is pressurised, the frictional torque (black line) increases over time until it reaches a peak. The rotational speed (grey line) remains at zero while the frictional torque reaches its maximum value. In the area of the drop in the frictional torque, the rotation of the shaft begins. Both graphs show similar characteristics up to the peak point. When the shaft begins to accelerate, the frictional torque rapidly decreases in a short amount of time. In the papers of San Andrés et al. [6] and Rudloff et al. [5], the frictional torque reached a local minimum after the bearing became airborne. The torque in Figure 6b shows a similar behaviour as that seen in these works, but in contrast, the torque does not increase after the lift-off event. An even larger deviation in the behaviour after lift-off is presented in Figure 6a. For the configuration with a $105\ \mu\text{m}$ clearance, a further decrease in the friction torque is detectable. Furthermore, the torque after lift-off does not show a local minimum. The minimum after the bearing becomes airborne was used as a criterion by San Andrés [6] to determine the lift-off speed. It is not possible to name the exact reason for these differences, as there are a number of factors (e.g., temperature or material relaxation) that can influence the behaviour after lift-off. These factors will be discussed in Section 4.

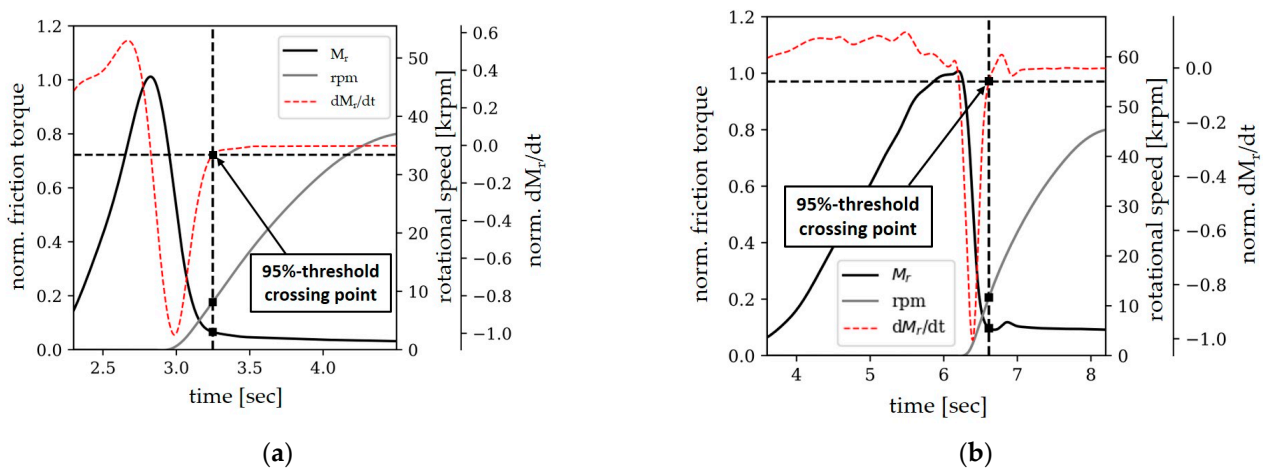


Figure 6. Test results from the friction torque measurements. Frictional torque (black line); rotational speed (gray line); time derivative of the frictional torque (red dashed line); (a) nom. clearance $105\ \mu\text{m}$ static load: 10 N; (b) nom. clearance $25\ \mu\text{m}$ static load: 70 N; ($1\ \text{krpm} = (100/3)\pi \cdot \text{rad/s}$).

Due to the absence of a local minimum, another criterion was defined. In Figure 6, the time derivative of the normalised friction torque (red dashed line), also normalized by its maximum absolute value, is also displayed with the measured signals. The normalised time derivative increases as the turbine becomes pressurised until the shaft begins to accelerate. During the transition phase from static to air friction, the derivative forms a downward peak. After lift-off, the change in frictional torque is much slower, despite the rapidly increasing rotor speed. The fallback of the time derivative is used to find a criterion when the lift-off has finished. In the following, a 95% fallback of the derivative after the downward peak is defined as a criterion. As shown in Figure 6, this level is arbitrary, but very practical. Its application detects the lift-off region very well.

3.3. Lift-Off Results

The explained criterion was used for all twenty bearing and load configurations. The determined load-dependent lift-off speeds are presented in Figure 7.

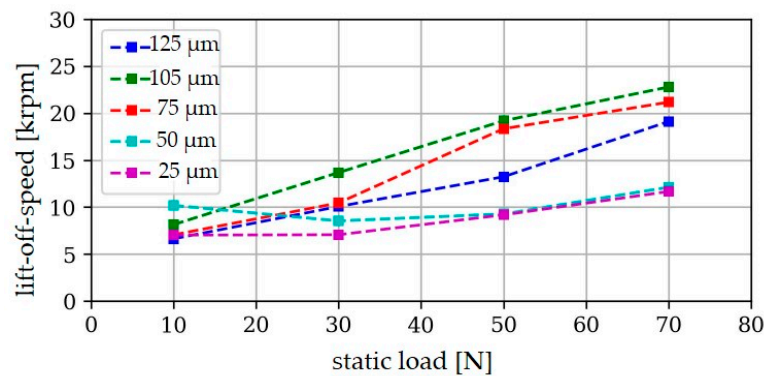


Figure 7. Illustration of the determined lift-off speeds (krpm) depending on the applied static load (N) for the bearing configurations with the nominal clearances; (blue: 125 μm), (green: 105 μm), (red: 75 μm), (turquoise: 50 μm), and (purple: 25 μm); (1 krpm = $(100/3)\pi \cdot \text{rad/s}$).

For the configurations with a nominal gap of 125 μm (blue), 105 μm (green), and 75 μm (red), the lift-off speed increases almost linearly with the static load. In contrast, for the two configurations with a nominal gap of 50 and 25 μm, the lift-off speed does not increase for all the measured loads. It is also notable that the lift-off event for the 50 μm gap configuration with a static load of 10 N occurs at a higher rotational speed than for the other configurations. In this study, the 105 μm configuration has the highest lift-off-speed values for all the loads. The only exception is the 10 N load case, in which the lift-off speed of the 50 μm configuration is higher than that of the others. The 10 N load case shows a different lift-off order than for the other load cases and is discussed separately.

For the 105, 75, 50, and 25 μm configurations, the lift-off speed decreases with the clearance. A decrease is also detectable between the 105 and the 125 μm configuration, implying that the load capacity has a minimum value in the investigated range.

Another view of the data is shown in Figure 8. The graphs show the determined lift-off speeds for each static load with the nominal clearance as the abscissa. For each specific load, the lift-off speed is non-linear as a function of the clearance. This non-linear behaviour becomes more dominant as the load increases and indicates a maximum in the clearance range of around 105 μm. In contrast to the other load cases, the lift-off speed with a 10 N static load does not change significantly, except for the 50 μm variant.

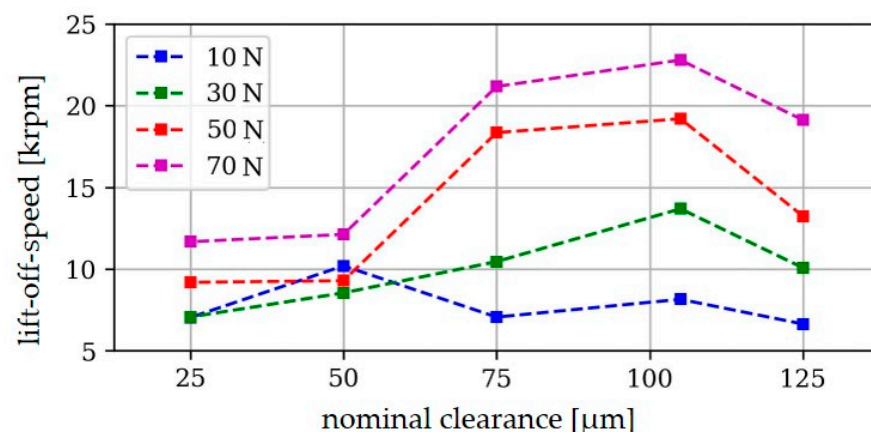


Figure 8. Illustration of the determined lift-off speeds (krpm) for each bearing configuration and the corresponding nominal clearance (μm) depending on the applied static load (N); (blue: 10 N), (green: 30 N), (red: 50 N), and (purple: 70 N); (1 krpm = $(100/3)\pi \cdot \text{rad/s}$).

The results shown so far provide information on the load at which the rotor starts to move, which allows the load capacities to be compared. The results of a linear regression are shown in Figure 9a. The slope of the straight line indicates the amount of load that

can be carried by each type of gap per revolution. In Figure 9b, these gradients are shown above the gap. The load-carrying capacity of the bearings increases more with the rotational speed for small gaps than for the larger gap configurations. It is interesting to see that in contrast to the measurements of Radil et al. [3], an optimal value for the bearing clearance does not exist. Instead, the gradients of the regression graphs show a minimum in the gap range of 75 μm . The results will be further discussed in Section 4.3.

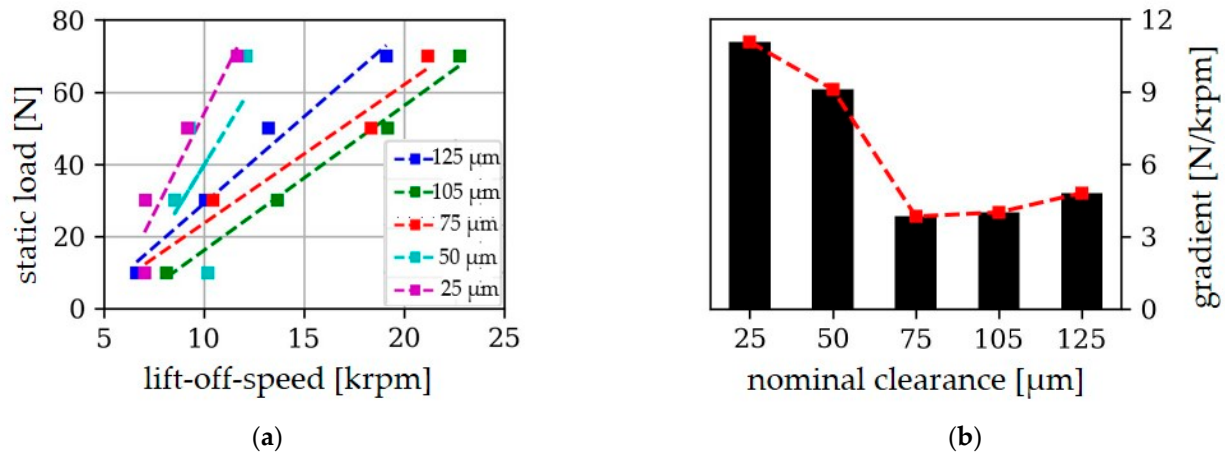


Figure 9. Results of a linear regression for each gap configuration; (a) lift-off data and linear regression (blue: 125 μm), (green: 105 μm) (red: 75 μm), (turquoise: 50 μm), (purple: 25 μm), (1 krpm = $(100/3)\pi \cdot \text{rad/s}$); (b) gradients of the linear regression for each different clearance configuration.

4. Discussion

4.1. Methodology

In this paper, two measurement concepts were described and used to investigate gas polymer bearings. The determination of the nominal gap via force–displacement or stiffness–displacement curves is common, as already mentioned in Section 2.2, and has been used by various research groups for several years. Although it is the standard, its validity should be discussed again at this point. In contrast to bearings with a rigid bearing wall, whose stiffness is high enough that contact-based measurement methods can be used without causing significant deformations, a different approach must be taken due to the elastic bearing wall. The use of non-contact measuring methods is also only suitable to a limited extent, as it would have to be ensured that all components of the elastic structure are in full contact. Since this is not guaranteed for bearings without preloading, the explained measuring method is used in the area of gas foil bearings. Due to the compliance of the elastic properties of the structure, the force does not increase infinitely faster after contact is reached. This means that for stiff structures, a change in the threshold value used has a smaller effect on the determined bearing gap than that for more compliant structures. It should also be taken into account that influences such as frictional forces in the contact surfaces of the bearing seats or bending moments due to weight forces, as well as alignment errors, have an effect on the measured curves. Table 2 shows the results of the measurement for all angular positions, as well as the mean value and the average value $(h_{\max} + h_{\min})/2$ of the measured interval of the results.

Table 2. Results of the bearing gap measurements for the six bearing configurations. The bold values equal to the measured clearances with the maximum distance to the interval average.

Adj. Foil [μm]	0°–180° [μm]	30°–210° [μm]	60°–240° [μm]	90°–270° [μm]	120°–300° [μm]	150°–330° [μm]	Mean [μm]	$(h_{\max} + h_{\min})/2$ [μm]	Nom. h_0 [μm]
0	122	110	120	114	140	132	122.83	124.5	125
20	100	110	116	95	95	100	102.667	105.5	105
50	77	70	80	82	81	83	78.83	76.5	75
75	60	52	45	53	61	52	53.92	53	50
100	26	29	20	27	27	30	26.92	25.5	25

The bold values in Table 2 are measured clearances with the greatest deviation from the measured interval average. The maximum deviation for all configurations is around 10%. Due to the fact that all the bearing configurations consist of the same components, except for the high precision adjustment foils, a deviation of ~10% can be interpreted as a kind of accuracy of the measurement method in this specific case.

The second method that was used in this work was the 95% fallback method. This method was introduced due to the absence of a minimum after the lift-off in some test cases. This minimum has been used by other researchers to determine the lift-off speed, e.g., San Andres [6]. Other groups of researchers, such as Zhou et al. [18], have used the deceleration phase to determine the lift-off speeds. A rapid change in the deceleration rate was the determination criterion in their paper. With the exception of the minimum criterion in the friction torque, the determination of the lift-off speed in the literature is generally based on the definition of a changing rate or threshold value in the measured friction torque or rotational speed. The choice of this value is subjective and has an influence on the results. The method of 95% fallback used in this work has been proven to be practicable according to a visual check across all the measured test cases in this study. However, the authors would like to point out that the results of this publication as well as the results of other lift-off measurements only reflect the range of the lift-off, and possible deviations cannot be excluded. The sensitivity of the results with regards to the threshold level will be further discussed in Section 4.3. The absence of a minimum in the friction torque is addressed in more detail in Section 4.2.

4.2. Decreasing Friction Torque after Lift-Off

As mentioned before, the measurement results of the friction torque have to be discussed due to the further decrease in the friction torque after lift-off. Common aerodynamic bearings with a rigid inner wall have a minimum friction torque after leaving a dry friction/mixed friction state. This occurs when the rotor becomes airborne. From that point on, the shear stress in the air film increases with the rotational speed and a minimum exists in the transition phase. When the bearing wall is elastic, the characteristics can be different due to different effects. The first point that should be discussed is the temperature. Thermal material expansion can influence the bearing characteristics by increasing or decreasing the bearing clearance. In this specific study, this should not be relevant, due to the short test durations and the long cooling times. Another temperature-based effect that can lead to a decrease in the friction torque is the thermal softening of the polymer. The authors consider this effect as relevant in general for gas polymer bearings, but not in the context of this study because of the short test durations. The authors see relaxation processes within the elastic structure as the most plausible reason for the observed effect. This can either be due to the gradual reduction in friction (slippage) in the contact areas of the structural components or due to material relaxation, which is a typical characteristic of polymers. In Dellacorte et al. [19], a friction torque curve measured with a bump-type bearing with the same effect of decreasing friction torque was published. For steel foils, the material relaxation is not the driving factor but the friction relaxation is also a suitable explanation here. Nevertheless, this effect should be further investigated in future studies.

4.3. Load Capacity of GPBs

The presented results of the study show that the bearing gap has a significant influence on the lift-off speed and thus on the load-carrying capacity of GPBs. In order to obtain a better comparability to other load capacity measurements and estimations, the load capacity coefficients (*LCC*), with regards to the paper of Dellacorte et al. [1], were calculated for all investigated GPB configurations. The “rule of thumb” (ROT) formula presented in [1,3] was applied, where the variables correspond to the physical or geometrical parameters listed below.

$$LCC = \frac{F}{(LD^2\Omega)} \quad (1)$$

LCC—load capacity coefficient [N/(mm³·krpm)];

F—static load [N];

L—axial bearing length [mm];

D—bearing inner diameter [mm];

Ω —lift-off speed [krpm].

The calculated *LCC* values as well as their mean value are presented in Table 3. It should be mentioned that the values are presented in SI units as well as in the imperial unit system [lbs/(in³·krpm)] to allow a direct comparison to the coefficients published in the already mentioned papers.

Table 3. Calculated load capacity coefficients (*LCCs*), for all bearing clearance configurations in SI-units as well as in the imperial unit system (for better literature comparability).

Nom. h_0	LCC		
	[μm]	[N/(mm ³ ·krpm)]	[lbs/(in ³ ·krpm)]
25		8.844×10^{-4}	3.257
50		7.273×10^{-4}	2.678
75		3.070×10^{-4}	1.131
105		3.205×10^{-4}	1.181
125		3.849×10^{-4}	1.417

In reference [1], the authors presented an overview for different types of gas foil bearings to show how the load capacities have increased over the time due to further development. The main difference between all these bearing generations can be found in the specific structure implementations. The authors would like to increase the readability of the following section; for this reason, all comparisons of the *LCCs* with results from the literature are in (lbs·in⁻³·krpm⁻¹). The published *LCCs* for air bearings with a rigid inner wall are in the range of 0.24 up to 0.3. The first-generation bump-type gas foil bearings could reach an *LCC* up to 0.43, which corresponds to an increase of around 25%. The second generation of compliant foil bearings, in which changes in the structural design were implemented (e.g., circumferential splits or multiple bump layers), could achieve even higher *LCC* values in the range up to 0.6. The third generation had an *LCC* range of 0.8 up to 1.4. In this generation, the elastic foils were split in the axial direction or staggered, which allows more adaptability of the structure to the pressure field. The range of *LCCs* in this study was 1.131 up to 3.257. As mentioned in Section 4.1, the sensitivity for the threshold level of 95% should be further investigated. For this reason, the *LCC* values for different threshold levels were calculated and are presented in Figure 10. The *LCC* values show a relatively high dependency on the threshold level. The scattering of the coefficients is higher for the levels of 95% and 97% as for the other values.

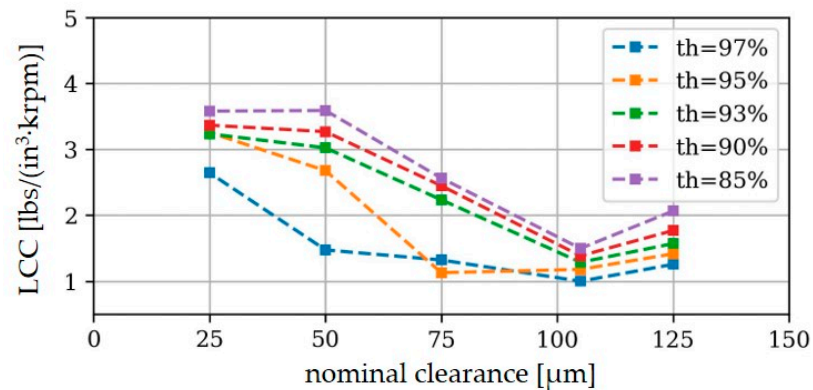


Figure 10. Load capacity coefficients (LCC) for different fallback threshold levels used for lift-off detection (blue: threshold level 97%), (yellow: threshold level 95%), (green: threshold level 93%), (red: threshold level 90%), (purple: threshold level 85%); (1 krpm = $(100/3)\pi \cdot \text{rad/s}$).

Nevertheless, it is worth noting that for all the cases presented, the LCCs are not above 1, and it can therefore be assumed that gas polymer bearings have carrying capacities that are comparable to those of gas foil bearings of the third generation. According to the authors, there are two main reasons that can explain the high values. Due to the more uniform distribution of the stiffness, as a result of the use of a continuous polymer layer:

- the adaptability of the structure to the shape of the pressure distribution in the gap is better than that with gas foil bearings of the first generation; and
- a thinner top foil can be used without a higher risk of sagging between the bumps, which also increases the adaptability of the structure.

Despite the strong sensitivity of the values determined with regards to the threshold value, it can be observed that the general characteristics are very similar for all cases. A comparison of the clearance study results published by Radil [3] shows a completely different behaviour. The LCC values of the investigated bump-type bearing (third generation) show an optimal value of the load-carrying capacity with regard to the bearing clearance. In contrast, the LCCs of the tested GPB configurations have a minimum but not a maximum that could be determined within the investigated clearance range. Unfortunately, there is no simple explanation for the observed differences. One possible reason could be the different measurement methods, but this cannot be confirmed with certainty. The influence of the temperature could also be a factor, as there was no thermal equilibrium on the test rig in this study. However, the results from Dellacorte et al. [1] contradict this. Here, the load capacities for a bearing were determined at 25 °C, 315 °C, and 650 °C. The LCC values were in the range of 0.8 to 1.0. This shows the dependency of the temperature, but from the authors' point of view, the differences in the LCC values, even at a temperature difference of ~300 °C, are too small to explain the differences observed in the LCC characteristics. Additionally, a significant temperature rise during the test was avoided by the short test durations and long breaks between the tests. In order to find an explanation for this issue, further investigations are necessary.

Another important result of this study is the further increase in the load capacity above the minimum. From the perspective of application design, this behaviour can offer an economic benefit. Due to the increasing tendency for higher clearances, the requirements for manufacturing tolerances can be reduced, which can reduce overall manufacturing efforts and the overall costs of an application. However, it should be noted that, due to the way aerodynamic bearings work, an indefinite increase in the bearing clearance is not possible. The actual value up to which the bearing gap can be increased depends on various factors. However, other publications (e.g., Sim et al. [10], Park et al. [11]) show that polymer bearings with bearing gaps of ~200 μm can also be used in high-speed operation and show good performance results.

5. Conclusions

In this study, the influence of a nominal bearing clearance on the load-carrying capacity of gas polymer bearings (GPBs) was investigated. For this purpose, a bearing prototype with a polymer layer made of NBR with a thickness of 2 mm and hardness of 50 Shore A was investigated. The bearing gap of the prototype was varied by high-precision adjustment foils. The nominal clearances were measured and discussed. The determined nominal clearances were 25, 50, 75, 105, and 125 μm . The accuracy of the method was estimated to be $\sim 10\%$.

In order to determine the lift-off speed, which is used to consider the load-carrying capacity, transient run-ups were carried out and the resulting frictional torque was measured. Frictional torque curves that differ from the classical journal bearing theory were observed. For some test cases, a further drop in the frictional torque was noticed after the lift-off. The authors attribute this to the presence of the elastic structure. For this reason, a very practical method for the determination of the lift-off was presented, in which a 95% fallback of the friction torque time derivative was used as a criterion. A sensitivity analysis for other threshold levels (85, 90, 93, 97%) was carried out. It was shown that for all threshold levels, the characteristic of the dependency was similar, but the calculated load capacity coefficients (LCCs) were highly dependent on the chosen threshold level. Nevertheless, the use of a 95% threshold level, which is one of the more conservative values leading to lower LCCs, showed good results for the load capacity for all GBP configurations. LCC values above $3.070 \times 10^{-4} \text{ N}/(\text{mm}^3 \cdot \text{krpm})$ ($1.131 \text{ lbs}/(\text{in}^3 \cdot \text{krpm})$) could be reached. The achieved LCC values are on the same level as those for third-generation bump-type bearings or even higher. From a load capacity perspective, this makes them suitable for practical applications in high-speed regimes (other aspects, such as dynamic stability and temperature resistance, especially of the polymers, must be considered as well).

Overall, the study was able to show that the influence of the bearing gap as a design parameter has a great impact on the load-carrying capacity of gas polymer bearings, with significant differences to the characteristics of bump foil bearings (minimum in the load capacity for clearances around 75 up to 105 μm) instead of an optimal value in the load capacity. Furthermore, the data show that the use of gas polymer bearings with larger bearing gaps may have a positive impact on the cost of machines due to a possible reduction in tolerance requirements. Additional benefits can also be gained from the simplicity of the bearing design. Unlike bump foils, the large scale production of polymer layers is already being carried out in other industries, such as in the manufacturing of seals. This allows existing scaling effects to be exploited, thus saving further costs.

Author Contributions: Conceptualization, G.S.; methodology, G.S.; software, G.S.; validation, G.S.; formal analysis, G.S.; investigation, G.S.; resources, R.L.; data curation, G.S. and R.L.; writing—original draft preparation, G.S.; writing—review and editing, R.L.; visualization, G.S.; supervision, R.L.; project administration, G.S.; funding acquisition, R.L. All authors have read and agreed to the published version of the manuscript.

Funding: This research received no external funding.

Institutional Review Board Statement: Not applicable.

Informed Consent Statement: Not applicable.

Data Availability Statement: Not applicable.

Conflicts of Interest: The authors declare no conflict of interest.

References

1. Dellacorte, C.; Valco, M.J. Load Capacity Estimation of Foil Air Journal Bearings for Oil-Free Turbomachinery Applications. *Tribol. Trans.* **2000**, *43*, 4. [[CrossRef](#)]
2. Heshmat, H. Advancements in the Performance of Aerodynamic Foil Journal Bearings: High Speed and Load Capability. *J. Tribol.* **1994**, *116*, 2. [[CrossRef](#)]

3. Radil, K.; Howard, S.; Dykas, B. The Role of Radial Clearance on the Performance of Foil Air Bearings. *Tribol. Trans.* **2002**, *45*, 485–490. [[CrossRef](#)]
4. San Andrés, L.; Chirathadam, T.A. A Metal Mesh Foil Bearing and a Bump-Type Foil Bearing: Comparison of Performance for Two Similar Size Gas Bearings. *ASME J. Eng. Gas Turbines Power* **2012**, *134*, 102501. [[CrossRef](#)]
5. Rudloff, L.; Arghir, M.; Bonneau, O.; Matta, P. Experimental Analyses of a First Generation Foil Bearing: Startup Torque and Dynamic Coefficients. *ASME J. Eng. Gas Turbines Power* **2011**, *133*, 092501. [[CrossRef](#)]
6. San Andrés, L.; Chirathadam, T.A.; Ryu, K.; Kim, T.H. Measurements of Drag Torque, Lift-off Journal Speed, and Temperature in a Metal Mesh Foil Bearing. *ASME J. Eng. Gas Turbines Power* **2010**, *132*, 112503. [[CrossRef](#)]
7. Hou, Y.; Xiong, L.-Y.; Chen, C.-Z. Experimental Study of a New Compliant Foil Air Bearing with Elastic Support. *Tribol. Trans.* **2004**, *47*, 308–311. [[CrossRef](#)]
8. Hou, Y.; Zhu, Z.-H.; Chen, C.-Z. Comparative test on two kinds of new compliant foil bearing for small cryogenic turbo-expander. *Cryogenics* **2004**, *44*, 69–72. [[CrossRef](#)]
9. Lee, Y.-B.; Kim, T.-H.; Kim, C.-H.; Lee, N.-S.; Choi, D.-H. Dynamic characteristics of a flexible rotor system supported by a viscoelastic foil bearing (VEFB). *Tribol. Int.* **2004**, *37*, 679–687. [[CrossRef](#)]
10. Sim, K.; Park, J. Performance Measurements of Gas Bearings with High Damping Structures of Polymer and Bump Foil via Electric Motor Driving Tests and One Degree-of-Freedom Shaker Dynamic Loading Tests. *ASME J. Eng. Gas Turbines Power* **2017**, *139*, 092504. [[CrossRef](#)]
11. Park, J.; Kim, D.; Sim, K. Development and Performance Measurements of Gas Foil Polymer Bearings with a Dual-Rotor Test Rig Driven by Permanent Magnet Electric Motor. *Appl. Sci.* **2022**, *12*, 1505. [[CrossRef](#)]
12. Park, J.; Sim, K. Rotordynamic Analysis of Gas Foil-Polymer Bearings Based on a Structural Elasticity Model of Polymer Layer along with Static-Load Deflection Tests. *Appl. Sci.* **2021**, *11*, 1789. [[CrossRef](#)]
13. Schilling, G.; Katja, B.; Liebich, R. Numerical Description of a Rotor Supported by Gas Polymer Bearings for Time Domain Simulations-Implementation and Parametrization of the Structure Model, 2018, SIRM 2019. In Proceedings of the 13th International Conference on Dynamics of Rotating Machines, Copenhagen, Denmark, 13–15 February 2019.
14. Kayo, C.; Liebich, R. Experimental Structural Analysis of Gas Foil Bearings. In *Mechanisms and Machine Science*; Springer International Publishing: Cham, Switzerland, 2018; pp. 264–280. [[CrossRef](#)]
15. Feng, K.; Liu, Y.; Zhao, X.; Liu, W. Experimental Evaluation of the Structure Characterization of a Novel Hybrid Bump-Metal Mesh Foil Bearing. *ASME J. Tribol.* **2016**, *138*, 021702. [[CrossRef](#)]
16. San Andrés, L.; Chirathadam, T.A.; Kim, T. Measurement of Structural Stiffness and Damping Coefficients in a Metal Mesh Foil Bearing. *ASME J. Eng. Gas Turbines Power* **2010**, *132*, 032503. [[CrossRef](#)]
17. Sim, K.; Yong-Bok, L.; Ho Kim, T.; Lee, J. Rotordynamic Performance of Shimmed Gas Foil Bearings for Oil-Free Turbochargers. *ASME J. Tribol.* **2012**, *134*, 031102. [[CrossRef](#)]
18. Zhou, Y.; Shao, L.; Zhao, S.; Zhu, K.; Ding, S.; Du, F.; Xu, Z. An Experimental Investigation into the Thermal Characteristics of Bump Foil Journal Bearings. *Symmetry* **2022**, *14*, 878. [[CrossRef](#)]
19. DellaCorte, C. A New Foil Air Bearing Test Rig for Use to 70WC and 70.000 rpm. *Trib. Trans.* **1998**, *41*, 335–340. [[CrossRef](#)]

Disclaimer/Publisher’s Note: The statements, opinions and data contained in all publications are solely those of the individual author(s) and contributor(s) and not of MDPI and/or the editor(s). MDPI and/or the editor(s) disclaim responsibility for any injury to people or property resulting from any ideas, methods, instructions or products referred to in the content.